

# High star formation rates as the origin of turbulence in early and modern disk galaxies

Green, Andrew W.<sup>1</sup>; Glazebrook, Karl<sup>1</sup>; McGregor, Peter J.<sup>2</sup>; Abraham, Roberto G.<sup>3</sup>; Poole, Gregory B.<sup>1</sup>; Damjanov, Ivana<sup>3</sup>; McCarthy, Patrick J.<sup>4</sup>, Colless, Matthew<sup>5</sup> & Sharp, Robert G.<sup>5</sup>

<sup>1</sup>*Centre for Astrophysics and Supercomputing, Swinburne University, PO Box 218, Hawthorn, VIC 3122, Australia*

<sup>2</sup>*Research School of Astronomy and Astrophysics, Australian National University, Cotter Rd, Weston, ACT 2611, Australia*

<sup>3</sup>*Department of Astronomy and Astrophysics, University of Toronto, 50 St George St, Toronto, ON M5S3H4, Canada*

<sup>4</sup>*Observatories of the Carnegie Institution of Washington, 813 Santa Barbara Street, Pasadena, CA 91101, USA*

<sup>5</sup>*Australian Astronomical Observatory, PO Box 296, Epping, NSW 1710, Australia*

**High spatial and spectral resolution observations of star formation and kinematics in early galaxies have shown that two-thirds are massive rotating disk galaxies<sup>1-5</sup> with the remainder being less massive non-rotating objects<sup>2,4,6-8</sup>. The line of sight averaged velocity dispersions are typically five times higher than in today's disk galaxies. This has suggested that gravitationally-unstable, gas-rich disks in the early Universe are fuelled by cold, dense accreting gas flowing along cosmic filaments and penetrating hot galactic gas halos<sup>9,10</sup>. However these accreting flows have not been observed<sup>11</sup>, and cosmic accretion cannot power the observed level of turbulence<sup>12</sup>. Here we report on a new sample of rare high-velocity-dispersion disk galaxies we have discovered in the nearby Universe where cold accretion is unlikely to drive their high star-formation rates. We find that the velocity dispersion is most fundamentally correlated with their star-formation rates, and not their mass nor gas fraction, which leads to a new picture where star formation itself is the energetic driver of galaxy disk turbulence at all cosmic epochs.**

Understanding how these different kinematic states of star-forming galaxies fit together is complicated by selection, surface-brightness and angular-resolution effects. Particularly at high redshift, resolution is a major limitation. The resolution gain of adaptive optics has enabled kinematic observations of early disks but not all observations, even within a particular survey, have taken advantage of adaptive optics<sup>2,4,8</sup>. Integral-Field Spectroscopy (IFS) (mainly of the H $\alpha$  emission line, which traces star formation and kinematics) has shallower surface-brightness limits than integrated spectroscopy. Kinematic observations are generally limited to the brightest (the char-

acteristic Schechter luminosity  $L^*$  or brighter<sup>5</sup>) high-redshift galaxies. Surface brightness is also a strong function of redshift (proportional to  $(1+z)^4$ ), and optical pass-bands commonly used for imaging sample the restframe-UV. These effects often complicate comparisons between the early and modern Universe. Finally, local IFS comparison samples are often selected from small volumes and non-uniformly.

To quantify how these difficulties might affect previous results, we turned to the well-studied Sloan Digital Sky Survey (SDSS) to put kinematic galaxy states in the context of a large, uniformly-selected sample. We undertook the first IFS observations of 65 star-forming<sup>13</sup> galaxies at redshift  $z \sim 0.1$ . As active galactic nuclei interfere with  $H\alpha$  emission as a star formation tracer, they have been excluded. (Further details of the selection criteria are in the Supplementary Information). Observed galaxies have  $H\alpha$  luminosities of  $10^{40.7}$  to  $10^{42.6}$  erg/s and median of  $10^{41.9}$  erg/s and stellar mass range and median of  $10^{9.1}$  to  $10^{10.9}$  and  $10^{10.3}$  solar masses, respectively<sup>14</sup>. Because only bright (which we shall define here as  $L_{H\alpha} > 10^{42}$  erg/s) objects are typically detected at  $z \sim 2$ , such objects make up half our observations despite representing only 3.2% of SDSS galaxies which otherwise meet our criteria. A broad selection illustrates the impact of surface brightness and luminosity on our results and those reported for the high-redshift Universe.

Chosen galaxies were observed using the integral-field spectrographs SPIRAL<sup>15</sup> on the 3.9m Anglo-Australian Telescope or WiFeS<sup>16</sup> on the ANU 2.3m telescope. Median seeing of 1.3" corresponds to a median spatial resolution of 2.3 kpc and the field of view is 10–40 kpc. This is closely matched to high-redshift samples observed with adaptive optics, but with better spectral resolution ( $\lambda/\Delta\lambda = 7000$  to 11,500). Following standard methods, we fit a Gaussian profile to the  $H\alpha$  emission-line spectrum at each spatial position in the reduced data cube. The free parameters of the fit are velocity dispersion (width, corrected for instrumental broadening), flux (height), and velocity (position). The velocity dispersion ( $\sigma$ ) is a simple, model-independent measure of the line-of-sight kinematics of a galaxy. Although there are many ways to measure it, we adopt the flux-weighted local mean definition commonly used at high redshift<sup>4,7,8</sup>:

$$\sigma_m = \frac{\sum \sigma_{\text{pix}} f_{\text{pix}}}{\sum f_{\text{pix}}} \quad (1)$$

where  $\sigma_{\text{pix}}$  is the standard deviation of the Gaussian fit to the  $H\alpha$  emission line in each spatial pixel, and  $f_{\text{pix}}$  is the  $H\alpha$  flux in that spatial pixel. This quantity measures the intrinsic velocity dispersion of the HII star forming regions and their random motions independent of large-scale systematic motions, such as rotation or orbital motion in a merger. Apparent velocity dispersion can also peak where systematic motions change abruptly, such as the bright central regions of a disk galaxy

where the velocity curve is steepest. We demonstrate that this does not affect our results in the Supplementary Information.

Unexpectedly, we find many disk-like velocity fields (Figure 1) with  $\sigma_m > 50$  km/s (high dispersion) among the galaxies with  $L_{H\alpha} > 10^{42}$  erg/s (high luminosity), very similar values to those at high redshift. We use two simple, qualitative criteria common to high-redshift analyses<sup>6</sup> to separate disks from non-disks based on their velocity and velocity-dispersion fields: (1) the velocity field must have a typical “spider diagram” shape, and (2) the velocity dispersion must be centrally peaked and fairly symmetric. Using these criteria all but six of our 17 objects at high dispersion and high luminosity are kinematic disks. The broad-band SDSS images also show most are disk galaxies, often with distinct bulges and disk components. This agrees with the picture that most of the star formation in the local Universe occurs in disks<sup>17</sup> and those disks forming stars most rapidly are kinematically hot, just as in the early Universe.

We compare the distribution of our galaxies in  $\sigma_m$  and  $H\alpha$  luminosity (shown in Figure 2) with several existing data sets from the early<sup>4,7,8</sup> and modern<sup>18–20</sup> Universe where  $\sigma_m$  has been measured in a comparable way (a summary of these data sets appears in the Supplementary Information). To check that surface-brightness dimming with redshift does not affect this comparison, we have applied redshift dimming (to  $z = 2.2$ ) and a surface-brightness limit ( $> 10^{16}$  erg/s/cm<sup>2</sup>/arcsec<sup>2</sup>, half that reported for OSIRIS<sup>7</sup>) to our data and recomputed  $\sigma_m$ . We find this affects our measure of  $\sigma_m$  by only 5–10 km/s. Furthermore, all of these comparison data sets fall within the stellar mass range of our data. Remarkably,  $\sigma_m$  appears to correlate with  $H\alpha$  luminosity above  $L_{H\alpha} = 10^{42}$  erg/s independent of redshift.

The  $H\alpha$  luminosity is directly correlated with the star-formation rate<sup>21</sup> (SFR). However, dust extinction in the galaxy can obscure some of this light, reducing the inferred SFR. Because dust-correction methods differ between authors, we use the observed quantity  $L_{H\alpha}$  to provide a simple, direct comparison between samples. In our sample, the mean flux ratio,  $H\alpha/H\beta = 4.13$  (based on SDSS fibre spectra) corresponds to a typical extinction at  $H\alpha$  of  $A_{H\alpha} = 0.78$  mag<sup>22</sup>. This correction has been included in the axis across the top of Figure 2 to give a rough scale to the star-formation rate for these galaxies.

Although primordial galaxies have been interpreted as turbulent gas-rich disks<sup>2,10</sup>, our results suggest gas density does not drive velocity dispersion. Applying the Kennicutt-Schmidt Law<sup>23</sup> to invert our star-formation surface densities into gas surface densities, we can estimate the gas-mass

fraction (relative to stars and gas) for these galaxies to range from 0.05 to 0.7 (median 0.18). The distributions of gas-fractions between high- and low-dispersion galaxies do not differ significantly, nor do the gas depletion timescales of 3–6 billion years. The wide range in gas fraction over a small range in luminosity is due to the wide range in stellar mass of these galaxies—stellar mass does not correlate with  $H\alpha$  luminosity. Figure 2 shows that there is no correlation between stellar mass and velocity dispersion. This implies star-formation rate is the important variable driving different velocity dispersions, not mass nor gas fraction, at all redshifts.

These high-dispersion galactic disks in the local Universe are an unexpected find. Continued detailed followup of these objects will shed more light on similar objects seen at high redshift. Cold-flow accretion is unlikely to be the origin of the high velocity dispersions as this mechanism is expected<sup>24</sup> to shut down rapidly for galaxies at  $z < 2$ . The high velocity dispersions in low-redshift galaxies then raise a question of whether cold-flow accretion is the appropriate mechanism for high velocity dispersions at high-redshifts. Recent absorption-line measurements have found no evidence for ubiquitous cold flows in the high-redshift Universe<sup>11</sup>. Our results suggest star formation itself powers the turbulence through energetic feedback. Indeed, simulations show that supernovae resulting from star formation can drive high velocity dispersions in the interstellar medium<sup>25</sup>.

It remains necessary to provide a mechanism to fuel the high star-formation rates of these galaxies. While the kinematics of our sample are not merger-dominated, there is evidence in the optical morphologies for minor-merger features such as small, close companions or tidal tails, many of which would be missed by current observations at high-redshift (e.g. panels f and j in Figure 1). Fresh gas brought in by these minor mergers may drive the high star-formation rates. These mergers could also inflate the velocity dispersions of the disks. The situation could be similar in the early Universe; the minor merger mechanism has been commonly invoked to drive the dramatic size evolution of red galaxies<sup>26</sup>, requiring minor mergers to occur frequently. Some of our objects also show companions at large distances with luminosity ratios between 1:2 to 1:3. This suggests gravitational tides could be compressing gas and inducing star-formation. Such a ‘fly-by’ mechanism would be considerably more important in the high-redshift Universe<sup>27</sup> (because of the high merger rate) and such objects could be massive, yet faint at optical wavelengths. Further study of the high-dispersion local galaxies is warranted to determine the physical mechanisms operating. These objects serve as rare reminders of the massive star formation that was so prevalent in the Universe 10 billion years ago.

1. Genzel, R. *et al.* The rapid formation of a large rotating disk galaxy three billion years after the Big Bang. *Nature* **442**, 786–789 (2006).
2. Förster Schreiber, N. M. *et al.* The SINS Survey: SINFONI Integral Field Spectroscopy of  $z \sim 2$  Star-forming Galaxies. *Astrophys. J.* **706**, 1364–1428 (2009).
3. Stark, D. P. *et al.* The formation and assembly of a typical star-forming galaxy at redshift  $z \sim 3$ . *Nature* **455**, 775–777 (2008).
4. Epinat, B. *et al.* Integral field spectroscopy with SINFONI of VVDS galaxies. I. Galaxy dynamics and mass assembly at  $1.2 < z < 1.6$ . *Astron. Astrophys.* **504**, 789–805 (2009).
5. Jones, T. A., Swinbank, A. M., Ellis, R. S., Richard, J. & Stark, D. P. Resolved spectroscopy of gravitationally lensed galaxies: recovering coherent velocity fields in subluminal  $z \sim 2-3$  galaxies. *Mon. Not. R. Astron. Soc.* **404**, 1247–1262 (2010).
6. Flores, H., Hammer, F., Puech, M., Amram, P. & Balkowski, C. 3D spectroscopy with VLT/GIRAFFE. I. The true Tully Fisher relationship at  $z \sim 0.6$ . *Astron. Astrophys.* **455**, 107–118 (2006).
7. Law, D. R. *et al.* The Kiloparsec-scale Kinematics of High-redshift Star-forming Galaxies. *Astrophys. J.* **697**, 2057–2082 (2009).
8. Lemoine-Busserolle, M., Bunker, A., Lamareille, F. & Kissler-Patig, M. 2D kinematics and physical properties of  $z \sim 3$  star-forming galaxies. *Mon. Not. R. Astron. Soc.* **401**, 1657–1669 (2010).
9. Dekel, A. *et al.* Cold streams in early massive hot haloes as the main mode of galaxy formation. *Nature* **457**, 451–454 (2009).
10. Elmegreen, B. G., Bournaud, F. & Elmegreen, D. M. Bulge Formation by the Coalescence of Giant Clumps in Primordial Disk Galaxies. *Astrophys. J.* **688**, 67–77 (2008).
11. Steidel, C. C. *et al.* The Structure and Kinematics of the Circum-Galactic Medium from Far-UV Spectra of  $z \sim 2-3$  Galaxies. *ArXiv e-prints* 1003.0679 (2010).
12. Elmegreen, B. G. & Burkert, A. Accretion-Driven Turbulence and the Transition to Global Instability in Young Galaxy Disks. *Astrophys. J.* **712**, 294–302 (2010).
13. Brinchmann, J. *et al.* The physical properties of star-forming galaxies in the low-redshift Universe. *Mon. Not. R. Astron. Soc.* **351**, 1151–1179 (2004).

14. Kauffmann, G. *et al.* Stellar masses and star formation histories for  $10^5$  galaxies from the Sloan Digital Sky Survey. *Mon. Not. R. Astron. Soc.* **341**, 33–53 (2003).
15. Sharp, R. *et al.* Performance of AAOmega: the AAT multi-purpose fiber-fed spectrograph. In *Society of Photo-Optical Instrumentation Engineers (SPIE) Conference Series*, vol. 6269 of *Presented at the Society of Photo-Optical Instrumentation Engineers (SPIE) Conference* (2006).
16. Dopita, M. *et al.* The Wide Field Spectrograph (WiFeS). *Astrophys. & Space Sci.* **310**, 255–268 (2007).
17. James, P. A., Knapen, J. H., Shane, N. S., Baldry, I. K. & de Jong, R. S. The H $\alpha$  Galaxy survey. IV. Star formation in the local Universe. *Astron. Astrophys.* **482**, 507–516 (2008).
18. Epinat, B., Amram, P. & Marcelin, M. GHASP: an H $\alpha$  kinematic survey of 203 spiral and irregular galaxies - VII. Revisiting the analysis of H $\alpha$  data cubes for 97 galaxies. *Mon. Not. R. Astron. Soc.* **390**, 466–504 (2008).
19. Epinat, B., Amram, P., Balkowski, C. & Marcelin, M. Evidence for strong dynamical evolution in disc galaxies through the last 11 Gyr. GHASP VIII - a local reference sample of rotating disc galaxies for high-redshift studies. *Mon. Not. R. Astron. Soc.* **401**, 2113–2147 (2010).
20. Tully, R. B. The Kinematics and Dynamics of M51. 1. the Observations. *Astrophys. J. S.* **27**, 415–435 (1974).
21. Kennicutt, R. C., Jr. Star Formation in Galaxies Along the Hubble Sequence. *ARA&A* **36**, 189–232 (1998).
22. Pei, Y. C. Interstellar dust from the Milky Way to the Magellanic Clouds. *Astrophys. J.* **395**, 130–139 (1992).
23. Kennicutt, R. C., Jr. The Global Schmidt Law in Star-forming Galaxies. *Astrophys. J.* **498**, 541–552 (1998).
24. Dekel, A. & Birnboim, Y. Galaxy bimodality due to cold flows and shock heating. *Mon. Not. R. Astron. Soc.* **368**, 2–20 (2006).
25. Dib, S., Bell, E. & Burkert, A. The Supernova Rate-Velocity Dispersion Relation in the Interstellar Medium. *Astrophys. J.* **638**, 797–810 (2006).
26. Glazebrook, K. Galaxy formation: Too small to ignore. *Nature* **460**, 694–695 (2009).

27. Menci, N., Fontana, A., Giallongo, E. & Salimbeni, S. Bimodal Color Distribution in Hierarchical Galaxy Formation. *Astrophys. J.* **632**, 49–57 (2005).
28. Lehnert, M. D., Heckman, T. M. & Weaver, K. A. Very Extended X-Ray and H $\alpha$  Emission in M82: Implications for the Superwind Phenomenon. *Astrophys. J.* **523**, 575–584 (1999).
29. Gilbank, D. G., Baldry, I. K., Balogh, M. L., Glazebrook, K. & Bower, R. G. The local star formation rate density: assessing calibrations using [OII], H and UV luminosities. *Mon. Not. R. Astron. Soc.* **405**, 2594–2614 (2010).

**Supplementary Information** is linked to the online version of the paper at [www.nature.com/nature](http://www.nature.com/nature)

**Acknowledgements** A.W.G and K.G. acknowledges financial support from the Australian Research Council. A.W.G. acknowledges a special scholarship from the Chancellery of the Swinburne University of Technology. We wish to thank the staff of the Anglo-Australian Observatory and the staff of the ANU 2.3m telescope for their support of these observations.

**Author Contributions** K.G. oversaw the project. A.W.G., K.G., I.D., P.J. McGregor, G.P. and R.G.S. collected the data at the telescope. A.W.G. completed the data reduction with help from P.J. McGregor and R.G.S. M.C. kindly provided observing time. A.W.G. and K.G. analysed the data and wrote the paper. All authors provided extensive suggestions and comments at each stage of the project.

**Competing Interests** The authors declare that they have no competing financial interests.

**Correspondence** Correspondence and requests for materials should be addressed to A.W.G. (via email: [agreeen@astro.swin.edu.au](mailto:agreeen@astro.swin.edu.au)).

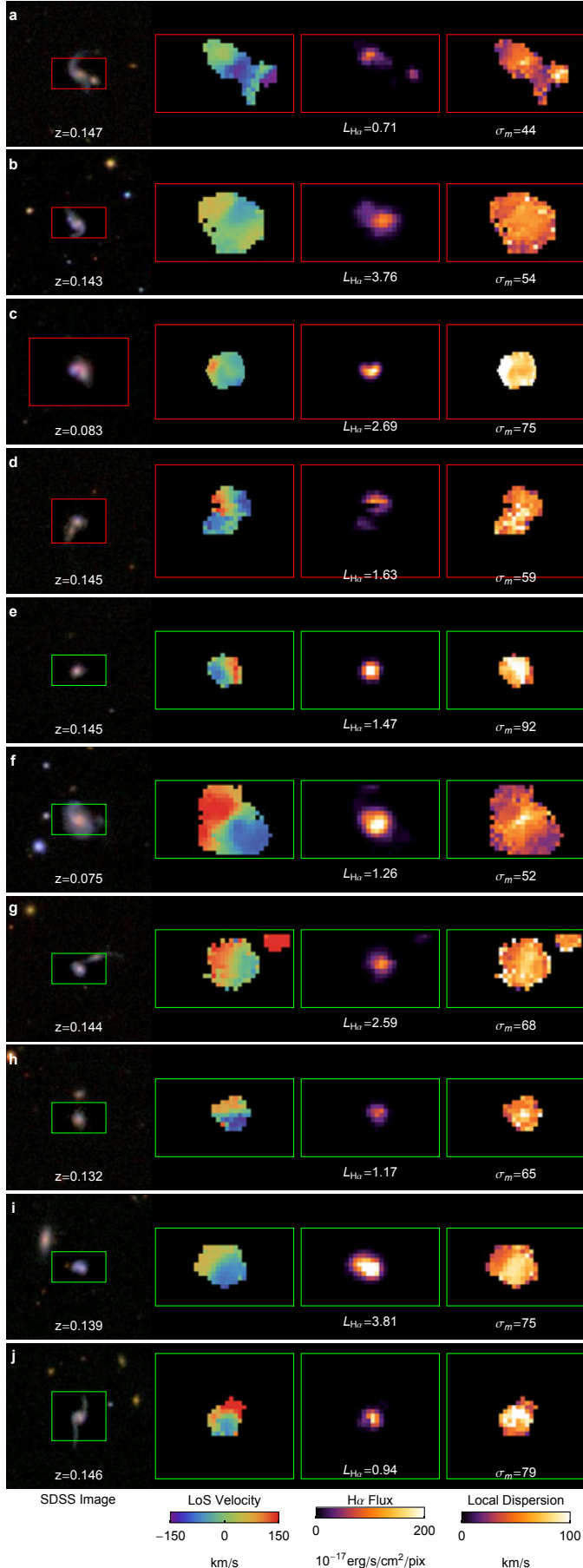


**Figure 1: Kinematic Pictures of Local galaxies**

All panels show the SDSS broadband image (red is  $\sim 750$ nm, green  $\sim 625$ nm and blue  $\sim 475$ nm), line-of-sight velocity map, H $\alpha$  narrowband image, and line-of-sight velocity dispersion map. All are scaled identically according to the scale at the bottom of the figure. The maps are masked when the emission-line fitting breaks down, typically at a  $4\sigma$  significance detection threshold. The green or red squares outline the field of view of the instrument in the images; red corresponds to non-disk objects and green to disk-like object. The broadband imaging of (a, b, and d) show clear merger activity, while (c) may have a merger axis close to the line of sight. Panel (a) shows a relatively small velocity dispersion, despite being a clear merger, suggesting that dispersion alone cannot distinguish mergers. Panels e-j are all objects with high dispersions ( $\sigma > 50$  km/s), but which are considered disks by our criteria. We emphasize these criteria are based on those typically employed on high-redshift observations<sup>6</sup>. (f) is a clear disk, with both a blue disk and a red bulge component visible in the broadband image. (g) shows a velocity gradient and a weak central dispersion peak. This galaxy's neighbour is 0.62 mag fainter, and has a similar radial velocity. The pair may ultimately become a major merger. (h) also has a companion which may or may not be at the same redshift. (i) shows two distinct clumps in the broadband image, indicative of a major merger, but still shows the clear kinematic characteristics of a disk. Finally (j) shows what one might argue is the signature of a disk in the kinematic data, but is a clear merger, with long tidal tails in the image. With the strong surface-brightness dimming with redshift, these tails would likely be invisible in a similar galaxy in the early Universe, and a disk interpretation would be made.



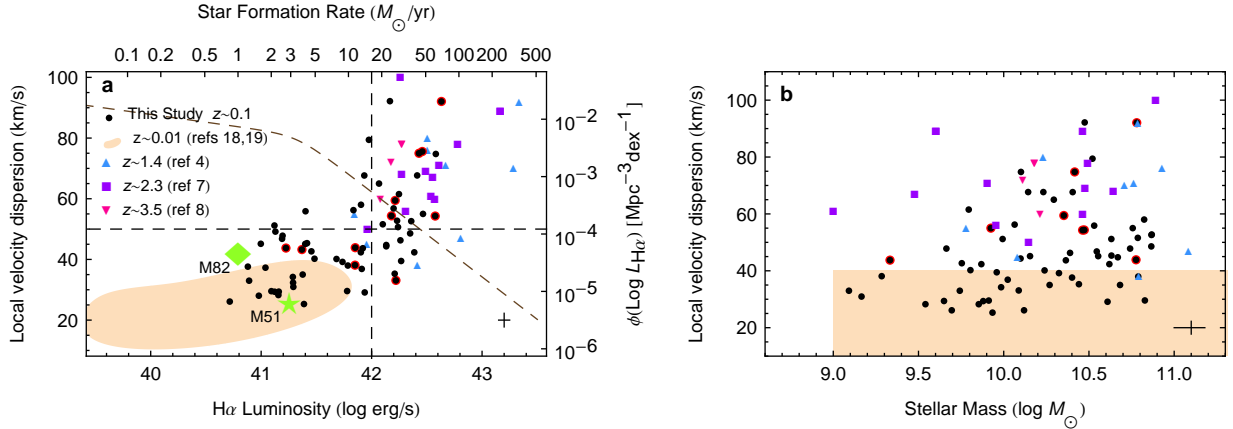


**Figure 2: Distribution of galaxy velocity dispersion against H $\alpha$  luminosity and stellar mass**

Panel (a) shows the distribution of flux weighted mean velocity dispersion and H $\alpha$  luminosity or star-formation rate of galaxies in our sample and comparison samples at  $z \sim 2^{4,7,8}$  and  $z < 0.01^{18,19}$ . The error bar in the lower right shows the combined, median errors. Velocity dispersion errors are typically  $\pm 5\text{--}10\%$  (systematic) and  $\pm 1\text{--}2$  km/s (statistical), and luminosity errors  $\pm 10\%$  (statistical). The variance and error in velocity dispersion are discussed in the Supplementary Information. Panel (b) shows the same, but plotted against stellar mass instead of H $\alpha$  luminosity. The points are labeled according to the key in panel (a). The comparison samples are described in the Supplementary Information. The positions of local galaxies M51<sup>20</sup> and M82<sup>28</sup> are labeled. Dashed lines at  $\sigma_m = 50$  km/s and  $L_{H\alpha} = 10^{42}$  erg/s separate the different regimes described in the text. Velocity dispersion appears to correlate with H $\alpha$  luminosity, but not mass. Non-disk galaxies are highlighted with red circles, and are not distinguishable by velocity dispersion or luminosity. The H $\alpha$  luminosity is derived from the full aperture of our data cubes so does not suffer from the large aperture effects common to SDSS fibre spectra.<sup>13</sup> The brown dashed line in (a) is the H $\alpha$  luminosity function of SDSS galaxies<sup>29</sup> with the scale on the right for comparison and shows the space density of star-forming galaxies declines sharply with higher luminosity.